Geophysical Research Letters

RESEARCH LETTER
10.1029/2025GL119487

Future Shoaling of the AMOC and Its Impact on Oceanic Heat Transport to the Subpolar North Atlantic

Sang-Ki Lee[1], Dongmin Kim[1,2], Hosmay Lopez[1], and Fabian A. Gomez[1,3]

[1]NOAA Atlantic Oceanographic and Meteorological Laboratory, Miami, FL, USA, [2]Cooperative Institute for Marine and Atmospheric Studies, University of Miami, Miami, FL, USA, [3]Northern Gulf Institute, Mississippi State University, Mississippi State, MS, USA

Key Points:

- Future weakening of the Atlantic Meridional Overturning Circulation (AMOC) is accompanied by significant vertical structural changes
- Specifically, suppressed deep-water formation leads to the AMOC's lower limb shoaling, causing it to carry warmer water southward
- This shoaling-induced reduction in thermal contrast between the AMOC's limbs accelerates the future weakening of oceanic heat transport

Supporting Information:

Supporting Information may be found in the online version of this article.

Correspondence to:

S.-K. Lee,
Sang-Ki.Lee@noaa.gov

Citation:

Lee, S.-K., Kim, D., Lopez, H., & Gomez, F. A. (2026). Future shoaling of the AMOC and its impact on oceanic heat transport to the subpolar North Atlantic. *Geophysical Research Letters*, *53*, e2025GL119487. https://doi.org/10.1029/2025GL119487

Received 15 SEP 2025
Accepted 20 DEC 2025

Author Contributions:

Conceptualization: Sang-Ki Lee
Formal analysis: Sang-Ki Lee
Investigation: Sang-Ki Lee, Dongmin Kim, Hosmay Lopez, Fabian A. Gomez
Methodology: Sang-Ki Lee, Dongmin Kim
Writing – original draft: Sang-Ki Lee
Writing – review & editing: Sang-Ki Lee, Dongmin Kim, Hosmay Lopez, Fabian A. Gomez

Abstract The Atlantic Meridional Overturning Circulation (AMOC) carries oceanic heat northward to the subpolar North Atlantic (SPNA), where the surface water cools and sinks to the deep ocean. According to a large-ensemble simulation under a medium-to-high emission scenario, the surface cooling and oceanic heat convergence in the SPNA may decrease to ∼20% of their historical levels by 2100. We show here that the projected weakening of the AMOC volume transport alone cannot explain such a large decrease in the heat convergence rate. Our analysis indicates that, due to the suppression of deep-water formation in the SPNA, the AMOC's lower limb becomes shallower, carrying relatively warm water southward away from the SPNA. This in turn accelerates the decrease in oceanic heat transport to the SPNA per unit AMOC weakening. These results are supported in other multi-ensemble models analyzed, despite large inter-model spreads.

Plain Language Summary The Atlantic Meridional Overturning Circulation (AMOC), often called the "ocean conveyor belt," plays a vital role in Earth's climate by carrying warm surface water from the tropics to the high-latitude North Atlantic. Here, the water cools, becomes denser, and sinks to the deep ocean, then returns south, effectively transporting oceanic heat northward. This system is crucial for regulating global weather patterns and climate. Our research, using advanced climate models, shows that in the future, increasing greenhouse gases will significantly reduce this northward oceanic heat transport. This happens not only because the AMOC conveyor belt itself weakens, but also because the deep southward flow becomes shallower (a process we call "shoaling"). As this deeper part of the conveyor belt shoals, it carries relatively warmer water southward. This change in the AMOC's vertical structure is crucial since it amplifies the overall reduction in heat transport to the high-latitude North Atlantic beyond what a simple weakening of the conveyor belt's strength would cause. Our findings highlight an accelerated reduction in oceanic heat transport to the high-latitude North Atlantic, with potential far-reaching consequences for global weather and climate.

1. Introduction

The Atlantic Meridional Overturning Circulation (AMOC) transports the upper Atlantic water masses (<1,000 m) northward (via the upper limb) and the deeper Atlantic water masses (>1,000 m) southward (via the lower limb), at a rate of ∼16.7 Sv (1 Sv ≡ 10^6 m^3 s^{-1}) across 26.5°N (e.g., Lee et al., 2024; Moat et al., 2020, 2023; Smeed et al., 2018). Since the upper water masses are much warmer than the deeper water masses, the AMOC transports ∼1.3 PW (1 PW = 10^{15} W) of ocean heat across 26.5°N. This heat is released to the atmosphere through vigorous air-sea interactions primarily in the subpolar North Atlantic Ocean (SPNA) (e.g., Ganachaud & Wunsch, 2000; Johns et al., 2011, 2023; Trenberth & Fasullo, 2017; Trenberth et al., 2019). Due to the extensive surface heat loss and the influx of saltier surface water from the subtropical North Atlantic (STNA), the upper water masses in the SPNA become heavier, and thus sink in and around the Labrador, Irminger and Nordic Seas, fueling the AMOC. This interplay between the AMOC heat transport and the surface cooling in the SPNA is a crucial component of the global ocean-atmosphere heat engine that regulates weather, climate, and ocean circulations.

As our planet warms, over 90% of the excess heat is absorbed by the ocean (e.g., Trenberth & Fasullo, 2010). Under a medium-to-high greenhouse gas emission scenario, the Community Earth System Model Version 2—Large Ensemble Simulation (CESM2-LENS; Rodgers et al., 2021) projects that the SPNA exhibits substantial excess heat uptake, reducing its rate of surface cooling by about 80% toward the end of the 21st century. This, combined with a similar rate of reduction in oceanic heat convergence in the SPNA, suggests a significant alteration in the global ocean-atmosphere heat engine (Figures 1a–1c). While concerning, a simple linear

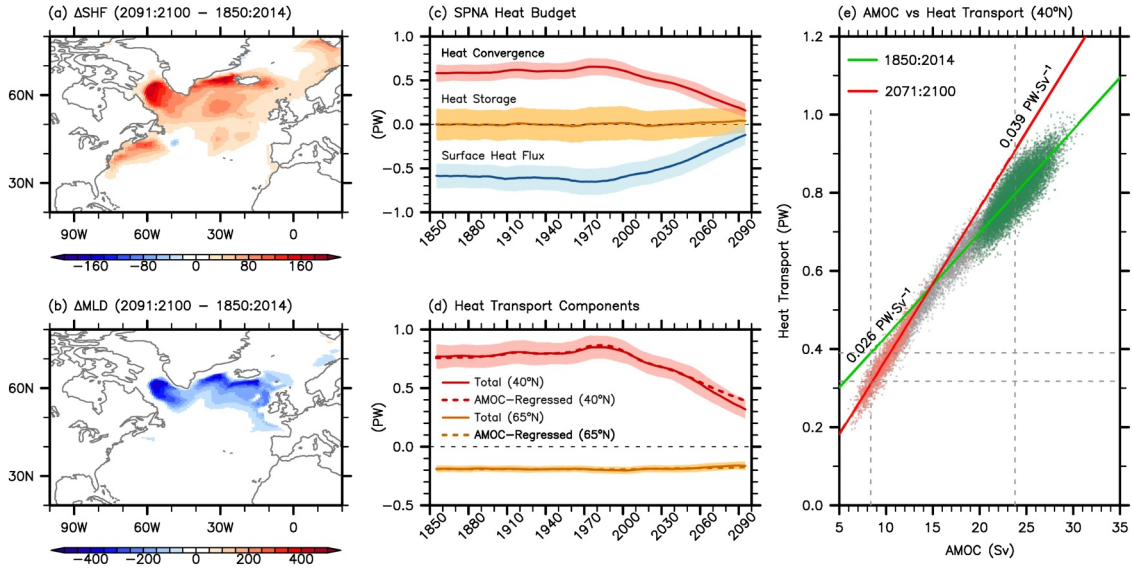

Figure 1. Changes in panel (a) the net surface heat flux (ΔSHF), which is positive downward, and (b) mixed layer depth (ΔMLD) from the historical period to the late 21st century, derived from CESM2-LENS. (c) Time series of heat budget terms (i.e., heat convergence, heat storage, and surface heat flux) for the SPNA (40°N–65°N), derived from CESM2-LENS. (d) Time series of OHT (solid lines) and that based on the relationship between the AMOC volume transport and OHT during the historical period (dashed lines) across 40°N and 65°N, derived from CESM2-LENS. (e) Scatterplot of the AMOC versus OHT across 40°N. The green, gray, and red dots indicate individual points (annually averaged) for HIST (1850–2014), 2015–2070, and 2071–2100, respectively derived from all 80 ensemble members of CESM2-LENS. The shaded error bands in panel (c, d) indicate that about 95% of the 80 ensembles reside within the error bands. The green line in panel (e) displays the linear regression for HIST, while the red line displays the linear regression for 2071–2100. The horizontal dashed lines in panel (e) indicate the OHT values for HIST and L21C (2091–2100), and the regressed OHT value based on HIST extrapolated to L21C. The vertical dished lines in panel (e) indicate the AMOC values for HIST and L21C. The units for ΔSHF, ΔMLD, and the heat budget terms for the SPNA are in W m^{-2}, m, and PW, respectively. The units for the AMOC volume transport and OHT are Sv, and PW, respectively.

regression based on the relationship between AMOC volume transport and oceanic heat transport (OHT) across 40°N during the historical period (1850–2014) suggests that the projected AMOC weakening alone cannot account for the extreme reduction in oceanic heat convergence in the SPNA (Figure 1d, solid and dashed red lines). This inconsistency, often overlooked in previous studies (e.g., Hankel, 2025; He et al., 2019; Li et al., 2022; Sévellec et al., 2017), suggests that as the AMOC slows down, it becomes less effective in transporting oceanic heat to the SPNA. Consequently, the future reduction in OHT to the SPNA may be accelerated beyond what is expected from the projected weakening of the AMOC volume transport alone, implying a greater disruption to the global climate and weather system.

The main goal of this study is to explore this apparent acceleration in the future decline of OHT to the SPNA in CESM2-LENS and to identify the physical processes contributing to it. In the following sections, after briefly introducing CESM2-LENS and other modeling tools used, we investigate the nonlinearity between AMOC volume and heat transports, and discuss the future shoaling of the AMOC's lower limb as the primary driver. Finally, we analyze four additional multi-ensemble climate models to verify the proposed mechanism, and then present a schematic summary of our major findings.

2. Models

We used CESM2-LENS (Rodgers et al., 2021) as our primary modeling tool to explore the future weakening of OHT to the SPNA and the associated nonlinearity in the relationship between the AMOC volume and heat transports. The AMOC, OHT, meridional velocity, ocean temperature, surface heat flux components, and mixed layer depth were derived for the historical period (1850–2014) and for the future period (2015–2100) under a medium-to-high end radiative forcing scenario of the Coupled Model Intercomparison Project Phase 6 (CMIP6) (i.e., Shared Socioeconomic Pathways 370; SSP-370). We used a total of 80 ensemble members from CESM2-LENS, initialized in 1850 from a preindustrial control simulation with four distinct states of the AMOC (strengthened, decreasing, weakened, and increasing). More detailed configurations of CESM2-LENS can be

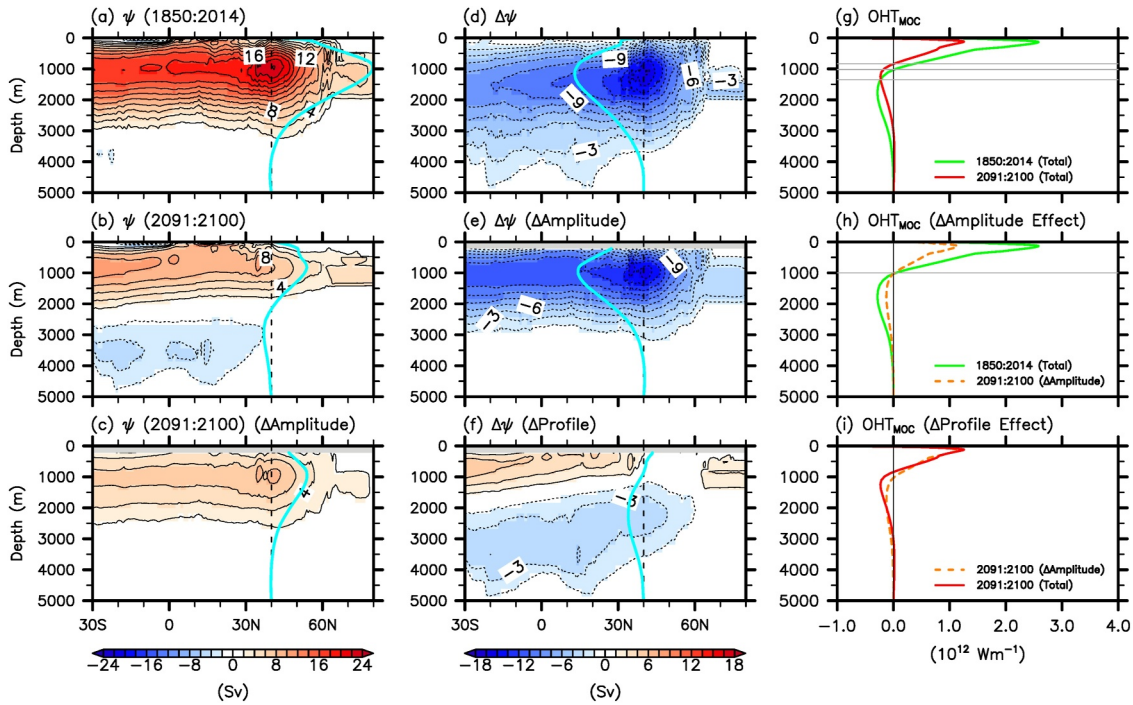

Figure 2. (a, b) The AMOC streamfunction averaged for (a) HIST and for (b) L21C. (c) The AMOC streamfunction with its amplitude (referenced at 40°N) weakened to the L21C level, but with no changes in the meridional-vertical profile. Panel (c) is computed by scaling the values in panel (a) by the fractional change in the maximum AMOC transport at 40°N from HIST to L21C. (d) The projected changes in the AMOC streamfunction from HIST to L21C, computed by subtracting (a) from (b). (e) The amplitude-only changes in the AMOC streamfunction, computed by subtracting (a) from (c). (f) The profile-only changes in the AMOC streamfunction, obtained by subtracting (c) from (b). (g–i) The vertical profiles of the AMOC heat transport (OHT_{MOC}) per unit depth at 40°N in HIST and L21C with (g) corresponding to (a, b), (h) corresponding to (a, c), and (i) corresponding to (b, c). The lines in panels (a–f) indicate the corresponding vertical profiles of the AMOC (or the AMOC changes) across 40°N. The AMOC streamfunction values in the upper 200 m in panel (c, e, f) are masked out because the wind-driven subtropical shallow overturning cell dominates in that depth range. The units are Sv for the AMOC volume transport, PW for the OHT, and 10^{-12} W m^{-1} for the OHT_{MOC} per unit depth.

found in Rodgers et al. (2021). The bias, variability, and externally forced response of the AMOC in CESM2-LENS were discussed in Lee et al. (2024).

In addition to CESM2-LENS, we also analyzed four sets of multi-ensemble CMIP6 model simulations under the historical and SSP-370 scenarios. They are UKESM1-0-LL (Sellar et al., 2019), CanESM5-1 (Sigmond et al., 2023), GISS-E2-1-G (Kelley et al., 2020), and MPI-ESM1-2-HR (Gutjahr et al., 2019). For each of these CMIP6 models, we analyzed 10 ensemble members.

3. Nonlinear Relationship Between the AMOC Volume and Heat Transports

To better understand the relationship between the AMOC volume transport and OHT to the SPNA, we regressed OHT at 40°N on the AMOC volume transport at the same latitude for two different periods, the historical period (1850–2014, HIST) and 2071–2100. As shown in Figure 1e, a −1.0 Sv reduction in the AMOC volume transport at 40°N leads to a −0.026 PW of OHT reduction during HIST (at the 95% confidence level of $\pm 3.0 \times 10^{-4}$ PW). During 2071–2100, the rate of OHT reduction increases to −0.039 PW per −1.0 Sv (at the 95% confidence level of $\pm 5.0 \times 10^{-4}$ PW). Therefore, the OHT across 40°N decreases much faster in the future than would be expected based on the linear relationship during HIST. These results support our hypothesis that the AMOC becomes less effective in transporting oceanic heat to the SPNA as it slows down.

4. What Makes the Future AMOC Less Effective in Transporting Oceanic Heat?

An important question is what causes the future AMOC to become less effective in transporting oceanic heat to the SPNA. We address this by examining the AMOC's spatial pattern in a meridional-vertical plane for HIST (Figure 2a) and for the late 21st century (2091–2100, L21C; Figure 2b). It is clear that the projected changes involve not only volume transport but also the meridional-vertical structure. During HIST, the AMOC's lower

limb (i.e., the southward flow) extends from ~1,000 to ~4,000 m. During L21C, its lower limit is shifted upward to ~2,000 m. Concurrently, the abyssal AMOC cell, which transports cold, dense water from the Antarctic northward, is enhanced (from 0.3 Sv in HIST to 1.8 Sv in L21C at 40°N) and its upper limit shifts from ~4,000 to ~2,000 m.

The difference in the AMOC streamfunction between HIST and L21C (Figure 2d) is dominated by the large reduction in AMOC volume transport, making the shoaling of the AMOC's lower limb and the strengthening of the abyssal cell less apparent. To better illustrate the projected changes in the meridional-vertical AMOC pattern, we construct a hypothetical AMOC pattern (Figure 2c) with its volume transport at 40°N reduced by the total weakening (i.e., from 23.8 Sv in HIST to 8.3 Sv in L21C), while its meridional-vertical structure remains unchanged from that of HIST. This is achieved by multiplying the AMOC of HIST by 0.35. Subtracting this from the AMOC of HIST yields the amplitude-only changes (Figure 2e). Similarly, subtracting it from the AMOC of L21C yields the profile-only changes (Figure 2f). Figure 2f clearly shows the relative strengthening of the upper part of the AMOC's lower limb (1,000–2,000 m), and the relative weakening of the lower part of the AMOC's lower limb (>2,000 m).

These results imply that while the North Atlantic Deep Water (NADW) formation rate weakens overall in L21C (see Figure 1b), the formation rate of the lower NADW (>2,000 m) reduces faster than that of the upper NADW (1,000–2,000 m). This results in not only a weakening but also a shoaling of the AMOC in its lower limb. This suggests that deep convection in the SPNA produces relatively shallow and warm deep-water masses in the future (i.e., relatively more upper NADW than lower NADW). Consequently, the lower limb of the AMOC becomes shallower and carries warmer water southward. This shoaling impact on OHT becomes clearer when comparing the vertical profiles of the AMOC heat transport ($\mathrm{OHT}_{\mathrm{MOC}}$) per unit depth at 40°N between HIST and L21C (Figure 2g). A vertical integration of these profiles can be written as

$$\mathrm{OHT}_{\mathrm{MOC}}(y,t) = \rho_{\mathrm{sw}}\mathrm{cp}_{\mathrm{sw}}\int_{z_b}^{\eta}\int_{x_e}^{x_w}\hat{v}T\,dxdz \tag{1}$$

where $\hat{v}$ is zonally averaged meridional velocity, T is ocean temperature, ρ_{sw} is the density of sea water (1,026 kg m^{-3}), $\mathrm{cp}_{\mathrm{sw}}$ is the specific heat of sea water (3,996 J kg^{-1} K^{-1}), x_w and x_e indicate the eastern and western boundaries of the Atlantic Ocean, respectively, and η and z_b indicate the sea surface height and sea floor depth, respectively. Here, $\mathrm{OHT}_{\mathrm{MOC}}$ per unit depth refers to $\mathrm{OHT}_{\mathrm{MOC}}$ prior to the vertical integration.

Figure 2g shows that the northward AMOC heat transport between 800 and 1,000 m in HIST is reversed southward in L21C, and the southward AMOC heat transport between 1,000 and 1,400 m increases from HIST to L21C. Figure 2h compares $\mathrm{OHT}_{\mathrm{MOC}}$ per unit depth corresponding to the amplitude-only changes in the AMOC with that of HIST. Similarly, Figure 2i compares $\mathrm{OHT}_{\mathrm{MOC}}$ per unit depth corresponding to the amplitude-only changes in the AMOC with that of L21C. These figures show that the increase in southward AMOC heat transport between 800 and 1,400 m is due to an upward shift of the AMOC's lower limb (i.e., shoaling), not due to the AMOC volume transport decrease. In summary, as the AMOC slows down, its lower limb becomes shallower and transports warmer water southward, thereby enhancing the decrease in $\mathrm{OHT}_{\mathrm{MOC}}$ per unit decrease in the AMOC volume transport across 40°N.

5. AMOC Heat Transport Decomposition: Weakening Versus Shoaling Effects

Note that the decomposition of the changes in the AMOC and associated $\mathrm{OHT}_{\mathrm{MOC}}$ per unit depth shown in Figure 2 are for illustration only. The formal definition and quantification of $\mathrm{OHT}_{\mathrm{MOC}}$ components associated with the AMOC amplitude and profile changes are discussed next. First, we estimate the volume transport-weighted temperature difference between the northward and southward flows of the AMOC (T_{DIF}), which can be written as

$$T_{\mathrm{DIF}}(y,t) = \frac{\int_{z_b}^{\eta}\int_{x_e}^{x_w}\hat{v}T\,dx\,dz}{0.5\int_{z_b}^{\eta}\int_{x_e}^{x_w}|\hat{v}|\,dx\,dz} \tag{2}$$

where the denominator represents the northward volume transport, primarily via the upper limb of the AMOC. T_{DIF} for HIST ($\overline{T}_{DIF}$) at 40°N is estimated to be 8.7°C. It decreases to 7.0°C in L21C; thus, the change in T_{DIF} from HIST to L21C (T'_{DIF}) becomes −1.7°C. This reduction in T_{DIF} enhances the decrease in the AMOC heat transport per unit decrease in the AMOC volume transport across 40°N, supporting our main hypothesis.

The AMOC heat transport (OHT_{MOC}) can be decomposed into four different terms. Here, only the Eulerian mean component is considered:

$$OHT_{MOC} = \rho_{sw} cp_{sw} \left[\underbrace{\overline{V}\overline{T}_{DIF}}_{\overline{OHT}_{MOC}} + \underbrace{V'\overline{T}_{DIF}}_{OHT'_{MOC[amp]}} + \underbrace{\overline{V}T'_{DIF}}_{OHT'_{MOC[pro]}} + \underbrace{V'T'_{DIF}}_{OHT'_{MOC[cov]}} \right] \quad (3)$$

where V refers to the northward volume transport, overbarred variables indicate the averages of HIST, and primed variables indicate the differences between HIST and L21C (i.e., L21C – HIST). The first term in the right side is the Eulerian mean OHT_{MOC} averaged in HIST ($\overline{OHT}_{MOC}$). The second term represents the AMOC amplitude change effect ($OHT'_{MOC[amp]}$). The third term represents the effect of vertical profile changes in both temperature and the AMOC ($OHT'_{MOC[pro]}$). Since the changes in vertical temperature profile during the 21st century plays a relatively minor role (Text S1, Tables S1 and S2 in Supporting Information S1; Mecking & Drijfhout, 2023), this term largely represents the AMOC profile change (or shoaling) effect. The last term represents the covariance of the AMOC amplitude and profile changes ($OHT'_{MOC[cov]}$). The northward volume transport of HIST at 40°N ($\overline{V}$) is 21.2 Sv. Note that this value is slightly lower than the total AMOC (23.8 Sv) mainly because only the Eulerian mean component is used to compute $\overline{V}$, while the bolus (i.e., the covariance of velocity and isopycnal thickness) and sub-meso scale components are not accounted for. The volume transport decreases to 9.0 Sv in L21C, which is slightly higher than the total AMOC (8.3 Sv).

Applying these values along with V′ (−12.2 Sv), $\overline{T}_{DIF}$ (8.7°C), and T'_{DIF} (−1.7°C), $\overline{OHT}_{MOC}$ is estimated to be 0.76 PW. It is reduced to 0.26 PW in L21C; thus, the difference in OHT_{MOC} between HIST and L21C (OHT'_{MOC}) becomes −0.50 PW. The AMOC amplitude change component, $OHT'_{MOC[amp]}$, is −0.43 PW, while the AMOC profile change component, $OHT'_{MOC[pro]}$, is −0.15 PW. The covariance component, $OHT'_{MOC[cov]}$, is 0.08 PW. Therefore, the AMOC amplitude change ($OHT'_{MOC[amp]}$) accounts for about 86% of the total OHT_{MOC} reduction, while the AMOC profile change ($OHT'_{MOC[pro]}$) accounts for 30%. About 16% is recovered (i.e., an increase) by the covariance ($OHT'_{MOC[cov]}$). Therefore, the AMOC amplitude change is the dominant factor, but the AMOC profile change (shoaling) still accounts for a significant portion (30%) of the total OHT_{MOC} reduction.

Note that the total OHT is the sum of the AMOC heat transport component (OHT_{MOC}) and the ocean-gyre heat transport component (OHT_{GYR}), which can be written as

$$OHT_{GYR}(y,t) = \rho_{sw} cp_{sw} \int_{z_b}^{\eta} \int_{x_e}^{x_w} (v - \hat{v})\, T\, dxdz \quad (4)$$

However, the ocean gyre in the North Atlantic is weak at the boundary between the STNA and SPNA, and its contribution is typically much less than the AMOC's (e.g., Johns et al., 2011, 2023; McCarthy et al., 2015; Xu et al., 2016). Consistently, Figures S2 and S3 in Supporting Information S1 confirm the limited contribution of ocean-gyre to the upper 400 m, making it much smaller than the AMOC component. OHT_{GYR} has an overall negative relationship with OHT_{MOC}, indicating that the ocean-gyre component partly compensates for the future weakening of the AMOC heat transport (Mecking & Drijfhout, 2023).

6. What Causes an Extensive Reduction of Surface Cooling in the SPNA?

Next, we explore the excess surface heat uptake in the SPNA during L21C, and how it is linked to the accelerated future weakening of the AMOC heat transport. As Figures 3a–3f show, this anomalous surface heat uptake (i.e., reduced surface cooling) is largely caused by an extensive reduction in turbulent heat flux components (i.e., a reduction in latent and sensible heat loss to the atmosphere). This large reduction in turbulent heat flux to the

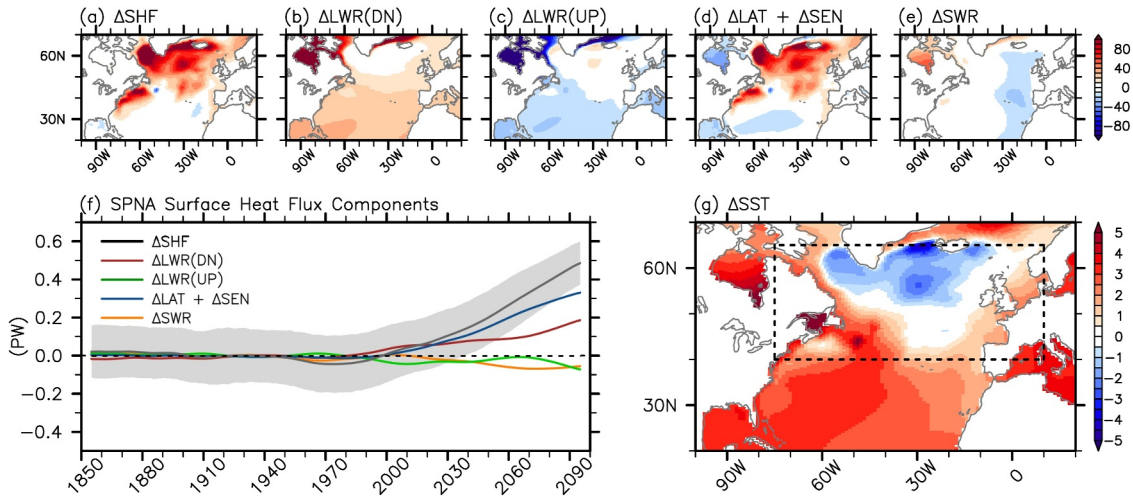

Figure 3. Changes in panel (a) net surface heat flux (ΔSHF), (b) downward longwave radiation (ΔLWR(DN)), (c) upward longwave radiation (ΔLWR(UP)), (d) latent and sensible heat flux (ΔLAT + ΔSEN), and (e) shortwave radiation (ΔSWR) from HIST to L21C, derived from CESM2-LENS. (f) Time series of the SPNA-integrated surface heat components, derived from CESM2-LENS. (g) Changes in SST from HIST to L21C, derived from CESM2-LENS. The shaded error band in panel (f) indicates the 95% limits of ΔSHF in the CESM2-LENS ensemble spread. Black dashed lines in panel (g) indicate the SPNA region. The sign convention for heat flux is positive downward. The units are W m^{-2} for the surface heat flux components in panels (a–e), PW for the SPNA-integrated heat flux components in panel (f), and °C for SST in panel (g).

atmosphere is supported by decreasing sea surface temperatures (SST) in the SPNA, a feature known as the warming hole (Figure 3g, e.g., Caesar et al., 2018; Chemke et al., 2020; Drijfhout et al., 2012; Park & Yeh, 2024; Rahmstorf et al., 2015; Robson et al., 2016).

Specifically, the warming hole, under rapidly rising air temperature and humidity, stabilizes the near-surface atmosphere (Figure S4 in Supporting Information S1), thereby reducing latent and sensible heat loss and driving the excess surface heat uptake in the SPNA. The weakening and shoaling of the AMOC greatly reduce oceanic heat convergence in the SPNA. This nearly offsets anomalous surface heat uptake (Figure 1c), preventing the SPNA from warming. This suggests that the future weakening and shoaling of the AMOC are key contributors to the warming hole, which in turn enables the excess surface heat uptake. Thus, the future weakening and shoaling of the AMOC, the warming hole, and the anomalous surface heat uptake are tightly coupled.

It should be noted, however, that the future weakening and shoaling of the AMOC are not directly driven by a decrease in OHT, but by surface freshening (due to land- and sea-ice melt), anomalous surface heat flux into the ocean, and the salt-advection feedback (e.g., Marotzke, 2000; Stommel, 1961; van Westen et al., 2024).

7. Discussion

One of the key remaining questions is whether the AMOC's lower limb shoaling and its impact on OHT are supported in other CMIP6 models. Figures S5–S8 in Supporting Information S1, which are analogous to Figures 1e and 2a–2f, show results for UKESM1-0-LL, CanESM5-1, GISS-E2-1-G, and MPI-ESM1-2-HR, respectively. These four CMIP6 models display a future shoaling of the AMOC's lower limb, consistent with CESM2-LENS (Figures 2a–2f). While the amplitude and vertical extent of the shoaling vary significantly among models, all four CMIP6 models also show that the AMOC becomes less efficient at transporting oceanic heat in 2071–2100 compared to that in HIST. This is evidenced by an increase in the slope (i.e., an increase in OHT per unit increase in the AMOC) in 2071–2100, despite a large inter-model spread (Text S2 in Supporting Information S1).

In agreement with these CMIP6 models, a weakened state of the AMOC often displays its shallower vertical structure in previous modeling studies (e.g., Danabasoglu et al., 2010, 2014; Msadek et al., 2013). However, CMIP6 models suffer from significant biases in the origins, properties and pathways of upper and lower NADW (e.g., Hirschi et al., 2020; Lee et al., 2019). For example, the present-day AMOC in CMIP6 models is often characterized by a lack of lower NADW (e.g., Bryden et al., 2024); thus, the rate of OHT reduction per unit

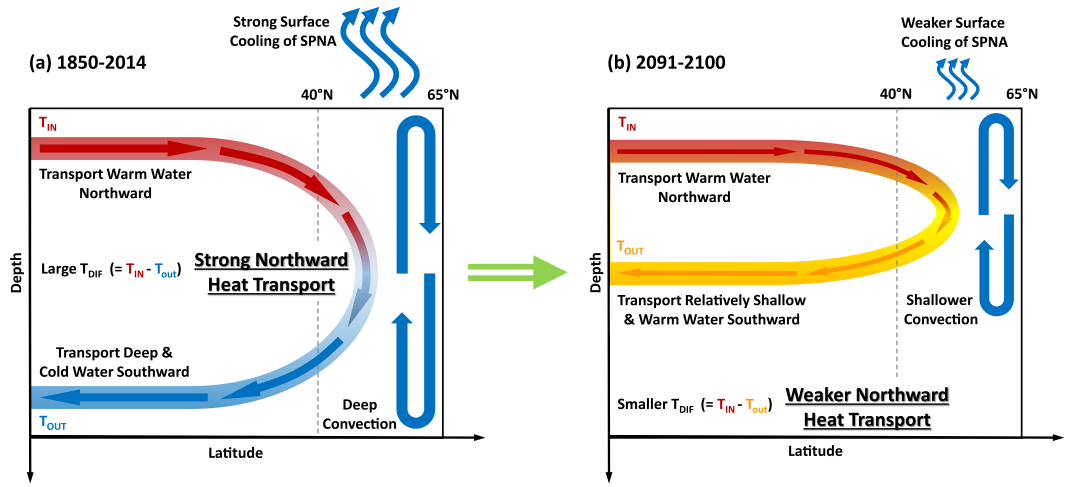

Figure 4. Summary schematic of the AMOC, OHT, deep convection, and surface cooling in the SPNA for (a) HIST (1850–2014), and for (b) L21C (2091–2100). The projected weakening of the AMOC reduces OHT to the SPNA at a rate proportional to the AMOC volume transport. Additionally, the future reduction in surface cooling over the SPNA leads to shallower deep-water convection and thus to a shoaling of the AMOC's lower limb, thereby promoting a warmer and shallower southward flow away from the SPNA. This in turn decreases the transport-weighted temperature difference between the upper and lower limbs of the AMOC (T_{DIF}), and thus further weakens OHT to the SPNA.

decrease in the AMOC is often smaller than the observed rate (Caesar et al., 2020; Johns et al., 2011, 2023), and the future weakening of the AMOC largely involves upper NADW. These biases may prevent models from correctly capturing the future shoaling of the AMOC's lower limb, leading to an underestimation of both the shoaling and its impact on OHT. Thus, improving model bias in simulating dense overflow waters from the Nordic Seas, their formation mechanisms, and pathways–the primary source of the lower NADW–is crucial (e.g., Chafik et al., 2025).

Finally, direct observation of the AMOC across 26.5°N shows that a decrease in the AMOC transport in its upper limb is largely countered by an opposite transport of the lower NADW. This directly leads to a shoaling of the AMOC's lower limb (e.g., Bryden, 2021; McCarthy et al., 2025; Smeed et al., 2014), which aligns with our main results. However, because the observed AMOC variability is predominantly interannual, a long-term trend of AMOC weakening (and shoaling) has not yet emerged above this interannual signal (e.g., McCarthy et al., 2025).

8. Conclusion and Summary

Our analysis of CESM2-LENS under a medium-to-high greenhouse gas emission scenario shows that both the surface cooling and oceanic heat convergence in the SPNA are projected to decrease toward ~20% of their historical levels by 2100. We demonstrate in this study that this cannot be achieved by the projected weakening of the AMOC volume transport alone. Thus, as the AMOC slows down in the future, it becomes less effective in transporting oceanic heat to the SPNA. In other words, the future weakening of OHT to the SPNA could be greater than that expected from the AMOC volume transport alone. Our novel OHT decomposition analysis indicates that the future shoaling of the AMOC's lower limb is mainly responsible for this difference.

Figure 4 illustrates the mechanism linking the shoaling of the AMOC's lower limb to the accelerated weakening of OHT to the SPNA. The weakening of the AMOC directly reduces OHT to the SPNA. Additionally, the future reduction in surface cooling over the SPNA leads to weaker and shallower convection, which promotes a warmer and shallower southward flow away from the SPNA. The shoaling of the AMOC's lower limb in turn decreases the volume transport-weighted temperature difference between the northward and southward flows of the AMOC (T_{DIF}), and thus further weakens OHT to the SPNA.

Conflict of Interest

The authors declare no conflicts of interest relevant to this study.

Data Availability Statement

All data used in this paper are publicly available. The CESM2-LENS data are available from Danabasoglu et al. (2020). For the multi-ensemble CMIP6 models UKESM1-0-LL, CanESM5-1, GISS-E2-1-G, and MPI-ESM1-2-HR, the historical scenario data are available from Tang et al. (2019), Swart et al. (2019a), NASA Goddard Institute for Space Studies (NASA/GISS) (2018), and Jungclaus et al. (2019), respectively. The corresponding SSP-370 scenario data are available from Good et al. (2019), Swart et al. (2019b), NASA Goddard Institute for Space Studies (NASA/GISS) (2020), and Schupfner et al. (2019).

Acknowledgments
The authors acknowledge Shenfu Dong, Denis Volkov, Rick Lumpkin, and Steve Yeager for helpful discussions. This work was supported by NOAA's Atlantic Oceanographic and Meteorological Laboratory, and carried out in part under the auspices of the Cooperative Institute for Marine and Atmospheric Studies, a cooperative institute of the University of Miami and NOAA, cooperative agreement NA 20OAR4320472. Fabian Gomez was supported by the Northern Gulf Institute under NOAA cooperative agreement NA21OAR4320190.

References

Bryden, H., Beunk, J., Drijfhout, S., Hazeleger, W., & Mecking, J. (2024). Comparing observed and modelled components of the Atlantic Meridional Overturning Circulation at 26°N. *Ocean Science*, *20*(2), 589–599. https://doi.org/10.5194/os-20-589-2024

Bryden, H. L. (2021). Wind-driven and buoyancy-driven circulation in the subtropical North Atlantic Ocean. *Proceedings of the Royal Society A*, *477*(2256), 20210172. https://doi.org/10.1098/rspa.2021.0172

Caesar, L., Rahmstorf, S., & Feulner, G. (2020). On the relationship between Atlantic meridional overturning circulation slowdown and global surface warming. *Environmental Research Letters*, *15*(2), 024003. https://doi.org/10.1088/1748-9326/ab63e3

Caesar, L., Rahmstorf, S., Robinson, A., Feulner, G., & Saba, V. (2018). Observed fingerprint of a weakening Atlantic Ocean overturning circulation. *Nature*, *556*(7700), 191–196. https://doi.org/10.1038/s41586-018-0006-5

Chafik, L., Årthun, M., Langehaug, H. R., Nilsson, J., & Rossby, T. (2025). The Nordic Seas overturning is modulated by northward-propagating thermohaline anomalies. *Communications Earth & Environment*, *6*(1), 573. https://doi.org/10.1038/s43247-025-02557-x

Chemke, R., Zanna, L., & Polvani, L. M. (2020). Identifying a human signal in the North Atlantic warming hole. *Nature Communications*, *11*(1), 1540. https://doi.org/10.1038/s41467-020-15285-x

Danabasoglu, G., Deser, C., Rodgers, K., & Timmermann, A. (2020). CESM2 large ensemble [Dataset]. *NSF National Center for Atmospheric Research*. https://doi.org/10.26024/kgmp-c556

Danabasoglu, G., Large, W. G., & Briegleb, B. P. (2010). Climate impacts of parameterized Nordic Sea overflows. *Journal of Geophysical Research*, *115*(C11), C11005. https://doi.org/10.1029/2010JC006243

Danabasoglu, G., Yeager, S. G., Bailey, D., Behrens, E., Bentsen, M., Bi, D., et al. (2014). North Atlantic simulations in coordinated ocean-ice reference experiments phase II (CORE-II). Part I: Mean states. *Ocean Modelling*, *73*, 76–107. https://doi.org/10.1016/j.ocemod.2013.10.005

Drijfhout, S., van Oldenborgh, G. J., & Cimatoribus, A. (2012). Is a decline of AMOC causing the warming hole above the North Atlantic in observed and modeled warming patterns? *Journal of Climate*, *25*(24), 8373–8379. https://doi.org/10.1175/JCLI-D-12-00490.1

Ganachaud, A., & Wunsch, C. (2000). Improved estimates of global ocean circulation, heat transport and mixing from hydrographic data. *Nature*, *408*(6811), 453–457. https://doi.org/10.1038/35044048

Good, P., Sellar, A., Tang, Y., Rumbold, S., Ellis, R., Kelley, D., & Kuhlbrodt, T. (2019). MOHC UKESM1.0-LL model output prepared for CMIP6 ScenarioMIP ssp370 [Dataset]. *Earth System Grid Federation*. https://doi.org/10.22033/ESGF/CMIP6.6347

Gutjahr, O., Putrasahan, D., Lohmann, K., Jungclaus, J. H., von Storch, J.-S., Brüggemann, N., et al. (2019). Max Planck Institute Earth System Model (MPI-ESM1.2) for the High-Resolution Model Intercomparison Project (HighResMIP). *Geoscientific Model Development*, *12*(7), 3241–3281. https://doi.org/10.5194/gmd-12-3241-2019

Hankel, C. (2025). The effect of CO_2 ramping rate on the transient weakening of the Atlantic Meridional Overturning Circulation. *Proceedings of the National Academy of Sciences of the United States of America*, *122*(1), e2411357121. https://doi.org/10.1073/pnas.2411357121

He, C., Liu, Z., & Hu, A. (2019). The transient response of atmospheric and oceanic heat transports to anthropogenic warming. *Nature Climate Change*, *9*(3), 222–226. https://doi.org/10.1038/s41558-018-0387-3

Hirschi, J. J.-M., Barnier, B., Böning, C., Biastoch, A., Blaker, A. T., Coward, A., et al. (2020). The Atlantic meridional overturning circulation in high-resolution models. *Journal of Geophysical Research: Oceans*, *125*(4), e2019JC015522. https://doi.org/10.1029/2019JC015522

Johns, W. E., Baringer, M. O., Beal, L. M., Cunningham, S. A., Kanzow, T., Bryden, H. L., et al. (2011). Continuous, array-based estimates of Atlantic Ocean heat transport at 26.5°N. *Journal of Climate*, *24*(10), 2429–2449. https://doi.org/10.1175/2010JCLI3997.1

Johns, W. E., Elipot, S., Smeed, D. A., Moat, B., King, B., Volkov, D. L., & Smith, R. H. (2023). Towards two decades of Atlantic Ocean mass and heat transports at 26.5°N. *Philosophical Transactions of the Royal Society A*, *381*(2262), 20220188. https://doi.org/10.1098/rsta.2022.0188

Jungclaus, J., Bittner, M., Wieners, K.-H., Wachsmann, F., Schupfner, M., Legutke, S., et al. (2019). MPI-M MPI-ESM1.2-HR model output prepared for CMIP6 CMIP historical [Dataset]. *Earth System Grid Federation*. https://doi.org/10.22033/ESGF/CMIP6.6594

Kelley, M., Schmidt, G. A., Nazarenko, L. S., Bauer, S. E., Ruedy, R., Russell, G. L., et al. (2020). GISS-E2.1: Configurations and climatology. *Journal of Advances in Modeling Earth Systems*, *12*(8), e2019MS002025. https://doi.org/10.1029/2019MS002025

Lee, S.-K., Kim, D., Gomez, F. A., Lopez, H., Volkov, D. L., Dong, S., et al. (2024). A pause in the weakening of the Atlantic meridional overturning circulation since the early 2010s. *Nature Communications*, *15*(1), 10642. https://doi.org/10.1038/s41467-024-54903-w

Lee, S.-K., Lumpkin, R., Baringer, M. O., Meinen, C. S., Goes, M., Dong, S., et al. (2019). Global meridional overturning circulation inferred from a data-constrained ocean & sea-ice model. *Geophysical Research Letters*, *46*(3), 1521–1530. https://doi.org/10.1029/2018GL080940

Li, Q., Luo, Y., & Liu, F. (2022). Asymmetric responses of the meridional ocean heat transport to climate warming and cooling in CESM. *Climate Dynamics*, *58*(3–4), 961–979. https://doi.org/10.1007/s00382-021-05948-w

Marotzke, J. (2000). Abrupt climate change and thermohaline circulation: Mechanisms and predictability. *Proceedings of the National Academy of Sciences*, *97*(4), 1347–1350. https://doi.org/10.1073/pnas.97.4.1347

McCarthy, G. D., Hug, G., Smeed, D., Morris, K. J., & Moat, B. (2025). Signal and noise in the Atlantic meridional overturning circulation at 26° N. *Geophysical Research Letters*, *52*(7), e2025GL115055. https://doi.org/10.1029/2025GL115055

McCarthy, G. D., Smeed, D. A., Johns, W. E., Frajka-Williams, E., Moat, B. I., Rayner, D., et al. (2015). Measuring the Atlantic meridional overturning circulation at 26°N. *Progress in Oceanography*, *130*, 91–111. https://doi.org/10.1016/j.pocean.2014.10.006

Mecking, J. V., & Drijfhout, S. S. (2023). The decrease in ocean heat transport in response to global warming. *Nature Climate Change*, *13*(11), 1229–1236. https://doi.org/10.1038/s41558-023-01829-8

Moat, B. I., Smeed, D. A., Rayner, D., Johns, W. E., Smith, R. H., Volkov, D. L., et al. (2023). *Atlantic meridional overturning circulation observed by the RAPID-MOCHA-WBTS (RAPID-Meridional Overturning Circulation and Heatflux Array-Western Boundary Time Series) array at 26N from 2004 to 2022 (v2022.1)*. British Oceanographic Data Centre - Natural Environment Research Council.

Moat, B. I., Smeed, D. A., Frajka-Williams, E., Desbruyères, D. G., Beaulieu, C., Johns, W. E., et al. (2020). Pending recovery in the strength of the meridional overturning circulation at 26°N. *Ocean Science*, *16*(4), 863–874. https://doi.org/10.5194/os-16-863-2020

Msadek, R., Johns, W. E., Yeager, S. G., Danabasoglu, G., Delworth, T. L., & Rosati, A. (2013). The Atlantic meridional heat transport at 26.5°N and its relationship with the MOC in the RAPID array and the GFDL and NCAR coupled models. *Journal of Climate*, *26*(12), 4335–4356. https://doi.org/10.1175/JCLI-D-12-00081.1

NASA Goddard Institute for Space Studies (NASA/GISS). (2018). NASA-GISS GISS-E2.1G model output prepared for CMIP6 CMIP historical [Dataset]. *Earth System Grid Federation*. https://doi.org/10.22033/ESGF/CMIP6.7127

NASA Goddard Institute for Space Studies (NASA/GISS). (2020). NASA-GISS GISS-E2.1G model output prepared for CMIP6 ScenarioMIP ssp370 [Dataset]. *Earth System Grid Federation*. https://doi.org/10.22033/ESGF/CMIP6.7426

Park, I. H., & Yeh, S. W. (2024). Projections of the North Atlantic warming hole can be constrained using ocean surface density as an emergent constraint. *Communications Earth & Environment*, *5*(1), 98. https://doi.org/10.1038/s43247-024-01269-y

Rahmstorf, S., Box, J. E., Feulner, G., Mann, M. E., Robinson, A., Rutherford, S., & Schaffernicht, E. J. (2015). Exceptional twentieth-century slowdown in Atlantic Ocean overturning circulation. *Nature Climate Change*, *5*, 475–480. https://doi.org/10.1038/nclimate2554

Robson, J., Ortega, P., & Sutton, R. (2016). A reversal of climatic trends in the North Atlantic since 2005. *Nature Geoscience*, *9*(7), 513–517. https://doi.org/10.1038/ngeo2727

Rodgers, K. B., Lee, S.-S., Rosenbloom, N., Timmermann, A., Danabasoglu, G., Deser, C., et al. (2021). Ubiquity of human-induced changes in climate variability. *Earth System Dynamics*, *12*(4), 1393–1411. https://doi.org/10.5194/esd-12-1393-2021

Schupfner, M., Wieners, K.-H., Wachsmann, F., Steger, C., Bittner, M., & Jungclaus, J. (2019). DKRZ MPI-ESM1.2-HR model output prepared for CMIP6 ScenarioMIP ssp370 [Dataset]. *Earth System Grid Federation*. https://doi.org/10.22033/ESGF/CMIP6.4399

Sellar, A. A., Jones, C. G., Mulcahy, J. P., Tang, Y., Yool, A., Wiltshire, A., et al. (2019). UKESM1: Description and evaluation of the U.K. Earth System Model. *Journal of Advances in Modeling Earth Systems*, *11*(12), 4513–4558. https://doi.org/10.1029/2019MS001739

Sévellec, F., Fedorov, A., & Liu, W. (2017). Arctic sea-ice decline weakens the Atlantic Meridional Overturning Circulation. *Nature Climate Change*, *7*(8), 604–610. https://doi.org/10.1038/nclimate3353

Sigmond, M., Anstey, J., Arora, V., Digby, R., Gillett, N., Kharin, V., et al. (2023). Improvements in the Canadian Earth System Model (CanESM) through systematic model analysis: CanESM5.0 and CanESM5.1. *Geoscientific Model Development*, *16*(22), 6553–6591. https://doi.org/10.5194/gmd-16-6553-2023

Smeed, D. A., Josey, S. A., Beaulieu, C., Johns, W. E., Moat, B. I., Frajka-Williams, E., et al. (2018). The North Atlantic Ocean is in a state of reduced overturning. *Geophysical Research Letters*, *45*(3), 1527–1533. https://doi.org/10.1002/2017GL076350

Smeed, D. A., McCarthy, G. D., Cunningham, S. A., Frajka-Williams, E., Rayner, D., Johns, W. E., et al. (2014). Observed decline of the Atlantic meridional overturning circulation 2004-2012. *Ocean Science*, *10*(1), 29–38. https://doi.org/10.5194/os-10-29-2014

Stommel, H. (1961). Thermohaline convection with two stable regimes of flow. *Tellus*, *13*(2), 224–230. https://doi.org/10.1111/j.2153-3490.1961.tb00079.x

Swart, N. C., Cole, J. N. S., Kharin, V. V., Lazare, M., Scinocca, J. F., Gillett, N. P., et al. (2019a). CCCma CanESM5.1 model output prepared for CMIP6 CMIP historical [Dataset]. *Earth System Grid Federation*. https://doi.org/10.22033/ESGF/CMIP6.17339

Swart, N. C., Cole, J. N. S., Kharin, V. V., Lazare, M., Scinocca, J. F., Gillett, N. P., et al. (2019b). CCCma CanESM5.1 model output prepared for CMIP6 ScenarioMIP ssp370 [Dataset]. *Earth System Grid Federation*. https://doi.org/10.22033/ESGF/CMIP6.17455

Tang, Y., Rumbold, S., Ellis, R., Kelley, D., Mulcahy, J., Sellar, A., et al. (2019). MOHC UKESM1.0-LL model output prepared for CMIP6 CMIP historical [Dataset]. *Earth System Grid Federation*. https://doi.org/10.22033/ESGF/CMIP6.6113

Trenberth, K. E., & Fasullo, J. T. (2010). Tracking Earth's energy. *Science*, *328*(5976), 316–317. https://doi.org/10.1126/science.1187272

Trenberth, K. E., & Fasullo, J. T. (2017). Atlantic meridional heat transports computed from balancing Earth's energy locally. *Geophysical Research Letters*, *44*(4), 1919–1927. https://doi.org/10.1002/2016GL072475

Trenberth, K. E., Zhang, Y., Fasullo, J. T., & Cheng, L. (2019). Observation-based estimates of global and basin ocean meridional heat transport time series. *Journal of Climate*, *32*(14), 4567–4583. https://doi.org/10.1175/JCLI-D-18-0872.1

van Westen, R. M., Kliphuis, M., & Dijkstra, H. A. (2024). Physics-based early warning signal shows that AMOC is on tipping course. *Science Advances*, *10*(6), eadk1189. https://doi.org/10.1126/sciadv.adk1189

Xu, X., Rhines, P. B., & Chassignet, E. P. (2016). Temperature–salinity structure of the North Atlantic circulation and associated heat and freshwater transports. *Journal of Climate*, *29*(21), 7723–7742. https://doi.org/10.1175/JCLI-D-15-0798.1